# Journal of Materials Chemistry A

Accepted Manuscript


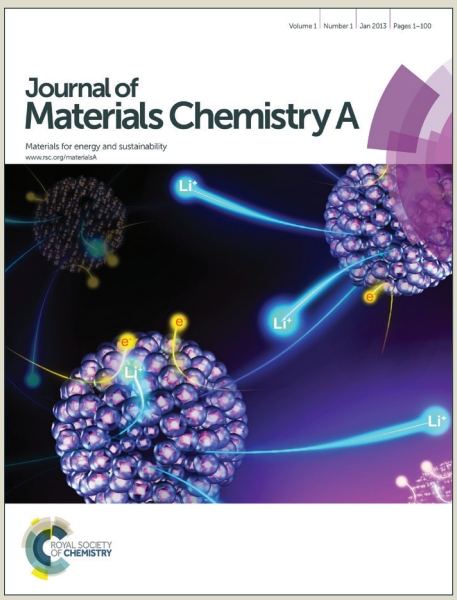





ROYAL SOCIETY OF CHEMISTRY

www.rsc.org/materialsA

# Direct synthesis of 3D hollow porous graphene balls from coal tar pitch for high performance supercapacitors

Xiaojun He [a,*], Hebao Zhang [a], Hao Zhang [a], Xiaojing Li [a], Nan Xiao [b], and Jieshan Qiu [b,*]

[a] School of Chemistry and Chemical Engineering, Anhui Key Lab of Coal Clean Conversion and Utilization, Anhui University of Technology, No. 59 Hudong Road, Maanshan 243002, China

[b] Carbon Research Lab, Liaoning Key Lab for Energy Materials and Chemical Engineering, State Key Lab of Fine Chemicals, Dalian University of Technology, Dalian 116024, China

**Abstract**

3D hollow porous graphene balls (HPGBs) are synthesized directly from coal tar pitch for the first time by a simple nano-MgO template strategy coupled with KOH activation. The as-made HPGBs feature 3D ball-like architecture with a thin porous shell consisting of macropores, mesopores and micropores in a well-balanced ratio, and have a high specific surface area. As the electrode material for supercapacitors, the as-made HPGBs show a high capacitance of 321 F $g^{-1}$ at 0.05 A $g^{-1}$ and an excellent rate performance of 244 F $g^{-1}$ at 20 A $g^{-1}$, and good cycle stability with over 94.4% capacitance retention after 1000 cycles. This work may pave a new way for efficient and scale-up production of low-cost ball-like graphene materials from aromatic hydrocarbon sources such as coal tar and heavy oils for supercapacitors.

Keywords: 3D porous graphene ball; direct synthesis; supercapacitor; high capacitance

*Corresponding authors. Telephone: +86-555-2312355. Fax: +86-555-2311822. E-mail address: agdxjhe@126.com (X.J. He); Telephone: +86-411-84986024. Fax: +86-411-84986015. E-mail address: jqiu@dlut.edu.cn (J. S. Qiu).

## Introduction

Supercapacitors have attracted increasing attention in recent years in view of their high charge-discharge rate, excellent stability and long cycle life. The electrochemical performance of supercapacitors depends on the electrode materials to a great degree. Carbon materials including porous graphitic carbon and carbon nanotubes are one of the main electrode materials for supercapacitors.[1–3] However, porous carbon-based supercapacitors suffer from electrode kinetic limitations because of the large ion-transfer resistance due to the long diffusion distance.[4–5] How to simultaneously achieve high power and large energy density for supercapacitors based on carbon materials remains a big challenge. Graphene is considered to be a potential electrode material of supercapacitors due to its good electronic conductivity, high electrochemical stability and large theoretical surface area.[6] However, the specific capacitance of graphene is far below its theoretical value because of the irreversible restacking of neighboring individual graphene sheet under working conditions due to the strong Van der Waals force.[7] This leads to a low specific surface area and seriously reduced electrochemical performance due to lacking of enough porous channels for fast transportation of electrolyte ions. 3D graphene has received particular attention for electrochemical energy storage and catalyst support due to its multidimensional electron transport pathways.[8–10] In particular, 3D Porous graphene (PG) with both large carbon network for high electronic conductivity and abundant channels for ion fast transportation is expected to have good rate performance and high capacitance.[11–14]

Up to now, the synthesis methods of graphene are mainly grouped into two kinds, i.e. "top-down" strategy,[15] and "bottom-up" strategy.[16,17] The "top-down" strategy involves the oxidation, exfoliation and activation of graphite, which is very complicated and hard to control due to the highly-bonded carbon network structures in graphite. The "bottom-up" strategy is based on the decomposition of carbon sources into the single carbon atom, and then the growth of graphene from the single carbon atom via chemical vapor deposition using

copper or other transition metals as a catalyst, which is also tedious and especially requires a precise control of experiment parameters. Recently, a solution deposition method was reported to synthesize novel 2D mesoporous graphene nanosheets via several steps including the synthesis of spherical carbon monomicelles, hydrothermal treatment, carbonization, and removal of anodic aluminum.[18] A one-step method combining ion-exchange and activation process was also reported to fabricate 3D hierarchical porous graphene-like material with metal ion-exchange resin as carbon precursor.[19] Nevertheless, the methods available now for PG production are time- and energy-consuming, resulting in high-cost PGs.

It is imperative to develop a simple and effective procedure for PG synthesis from cheap carbon sources. Coal tar pitch, a by-product of the coking process of coal industry, is cheap, abundant and in particular, has low ash content. The yearly production capacity of coal tar in China alone is over 20 million tons, of which over 50% is coal tar pitch. Coal tar pitch contains many polycyclic aromatic hydrocarbon molecules that can be regarded as small-sized graphene to some degree. Liquefied pitch prefers to be coated onto the surface of highly-dispersed template, resulting in a thin coating layer that can be transformed into graphene at high temperatures. Primitive graphene layers in parent coals have been investigated at molecular level.[20,21] The abundant polyaromatic structures with a narrow size distrubution in coal tar pitch are quite similar to $sp^2$ hybridization bonding structures in graphene. This makes it possible to directly synthesize PG from coal tar pitch. In the past decade, our group has made efforts to study the feasibility of fabricating graphene and porous carbon from coal and its derivatives.[22,23] It has been reported that nano-MgO can be used as template or catalyst in chemical vapor deposition processes for synthesis of graphene capsules, and can be easily removed by diluted acid,[24] and recovered by chemical precipitation method to make $MgCO_3$ and then MgO after the decomposition of $MgCO_3$. Here we report the synthesis of hollow porous graphene balls (HPGBs) directly from coal tar pitch using nano-sized MgO as template coupled with KOH activation. The as-made HPGBs from coal tar pitch in the present

work feature 3D hollow ball-like morphology with a porous thin shell. To our best knowledge, no reports about the direct production of HPGBs from coal tar pitch are available up to now.

## Experimental Section

### Synthesis of HPGBs

A coal tar pitch with a softening point of 383 K from Maanshan Ion & Steel Co. Ltd. of China was used as carbon precursor.[22] Other chemicals were purchased from Aladdin, and used as received. For a typical run, the mixture of coal tar pitch (3.0 g) with a particle size below 100 μm, nano-MgO (18.0 g) and KOH (6.0 g) was ground and mixed in solid state. The pulverized mixture was transferred to a corundum boat that was put into a tube furnace and heated to 423 K at 5 K $min^{-1}$ and kept for 30 min, and then heated to 1073 K and kept for 1 h in a flowing argon or nitrogen (60 mL $min^{-1}$) to make HPGBs. The HPGBs were washed by 2M HCl solution and distilled water to remove the inorganic impurities, and dried at 383 K for 24 h before use. The as-made HPGBs in argon and $N_2$ atmosphere are termed as $HPGB_{Ar}$ and $HPGB_{N2}$, respectively. For comparison, the pressure in the tube furnace was controlled in a range from −0.05 to −0.10 MPa in the heat treatment step. Before the heat treatment, the tube was flushed by flowing $N_2$ to get rid of air. The HPGB made at negative pressure from −0.05 to −0.10 MPa with a mass ratio of coal tar pitch, MgO, KOH remaining the same as that of $HPGB_{N2}$ (3.0 g of coal tar pitch, 18.0 g of MgO, 6.0 g of KOH) is termed as $HPGB_{NP-6}$, while the HPGB made with a mass of coal tar pitch, MgO, KOH at 4.2 g, 16.8 g, 6.0 g is termed as $HPGB_{NP-4}$. The carbon materials made under the same conditions in argon without addition of MgO or KOH are termed as porous carbon ($PC_{1Ar}$) and $HPGB_{2Ar}$. Before test and characterization, the as-made carbon materials were ground to a fine powder with a particle size below 44 μm.

### Structure characterization

The pore structure of HPGB was studied by $N_2$ adsorption-desorption at 77 K using ASAP2010. The BET surface area ($S_{BET}$) of HPGB was calculated by the BET

(Brunauer−Emmett−Teller) equation in a relative pressure range of 0.05 to 0.24. The pore size distribution was calculated by the density functional theory (DFT) method. The total pore volume ($V_t$) was obtained at a relative pressure of 0.99. The micropore volume ($V_{mic}$) was estimated by using the t-plot method. The mesopore volume ($V_{meso}$) was calculated from the difference of $V_t$ and $V_{mic}$. The average pore size ($D_{ap}$) of HPGB was obtained by the equation of $D_{ap}=4V_t/S_{BET}$. The microstructures of HPGB were examined by field emission scanning electron microscopy (FESEM, Nanosem430), transmission electron microscopy (TEM, JEOL, JEM−2100), and X-ray diffraction (XRD, Philips X, CuK radiation). The ash content in HPGB was determined by burning HPGB at 1173 K in flowing air of 30 mL $min^{-1}$ in a thermogravimetric analyzer (DTG−60, Japan). The chemical bonding states of carbon, oxygen and nitrogen elements in HPGB were analyzed by X-ray photoelectron spectroscopy (XPS, Thermo ESCALAB250, USA). The Raman spectra of HPGB were recorded on a Raman spectroscopy (JYLab−Ram HR800, excited by a 532 nm laser).

**Electrochemical test**

The electrodes were made by mixing HPGB (85.0 wt%) and polytetrafluoroethylene (15.0 wt%), and then pressed at 20.0 MPa for 10 s followed by drying at 383 K for 2 h under vacuum. A button-type supercapacitor was assembled with two similar carbon electrodes (about 5 mg $cm^{-2}$) separated by a polypropylene membrane in 6 M KOH electrolyte. The supercapacitors were evaluated by cyclic voltammetry (CV) on a CHI760C electrochemical workstation (CH Instrument, Shanghai, China). The charge-discharge performance of supercapacitors was measured on a supercapacitance test system (SCTs, Arbin Instruments, USA). The specific capacitance of HPGB electrode ($C$, in F $g^{-1}$) was calculated based on the discharge curve according to Eq. (1).

$$C = \frac{2I}{m\frac{\Delta V}{\Delta t}} \qquad (1)$$

where $I$ is the discharge current (A), $\frac{\Delta V}{\Delta t}$ (V $s^{-1}$) is the slope obtained by fitting a straight line to the discharge voltage, and $m$ is the mass (g) of active material in single electrode.

The energy density ($E$, in Wh $kg^{-1}$) and average power density ($P$, in W $kg^{-1}$) of supercapacitors were calculated according to Eq. (2) and (3).

$$E = \frac{1}{2 \times 4 \times 3.6} C V^2 \qquad (2)$$

$$P = \frac{E}{\Delta_{td}} \qquad (3)$$

where $C$ is the specific capacitance of single electrode in two-electrode supercapacitor (F $g^{-1}$), and $V$ is the usable voltage after IR drop (V), and $\Delta_{td}$ is the discharge time (h).

The specific capacitance of HPGB electrodes ($C$, in F $g^{-1}$) was also calculated from the CV curves according to Eq. (4).

$$C = \frac{2\int_{V_1}^{V_2} i(V)dV}{mv\Delta V} \qquad (4)$$

where $V_1$ and $V_2$ (V) are the lower and upper limit of potential in a cyclic potential sweep, respectively; $\Delta V = V_2 - V_1$, is the voltage window; $v$ is the scan rate (V $s^{-1}$); $i(V)$ is the current as the function of voltage, and $m$ is the mass (g) of active material in single electrode.

The electrochemical impedance spectroscopy (EIS) measurement was performed with an amplitude of 5 mV over a frequency of 100 kHz to 0.001 Hz using a Solartron impedance analyzer (Solartron Analytical, SI 1260, UK) with a Solartron potentiostat (SI 1287). The specific capacitance of HPGB electrodes ($C$, in F $g^{-1}$) was also obtained based on the EIS measurement by Eq. (5).

$$C = -\frac{4}{2\pi m f Z''} \qquad (5)$$

where $f$ is the frequency (Hz) and $Z''$ is the imaginary impedance (Ohm).

The surface area normalized capacitance $C_{sa}$ (μF $cm^{-2}$) was calculated by Eq. (6).[25]

$$C_{sa} = \frac{C}{S_{BET}} \times 100 \qquad (6)$$

where $S_{BET}$ is the specific surface area ($m^2\ g^{-1}$) derived from the $N_2$ adsorption and $C$ is the specific capacitance of the single electrode (in $F\ g^{-1}$).

**Results and discussion**

**Fig. 1** shows the schematic of the direct fabrication of HPGBs from coal tar pitch and the possible mechanism involved in the process. Coal tar pitch is liquefied at 423 K, and then coated onto the surface of nano-sized MgO particles to form thin coating layers made of aromatic hydrocarbons from coal tar pitch due to the template function of nano-MgO particles. Meanwhile, KOH mixed in the pitch in the grinding step is embedded in the thin coating layers. In the subsequent heating step, some gaseous products are formed *in situ* in the thin carbonaceous coating layers due to the decomposition of hydrocarbons. The coating layers are gradually transformed to thin carbon layers with a ball-like architecture because of the combined effect of internal gas pressure due to the decomposition and reorganization of hydrocarbons and the MgO template effect. At the same time, KOH is melted at about 653 K and diffused in the reactants after the temperature reaches the melting point of KOH. Subsequently, KOH embedded in the coating layers would activate the aromatic hydrocarbons at elevated temperatures to create pores with different sizes in the ball-like shells of thin carbon layers. The core-like MgO template and the K-containing compounds formed during this activation step are removed later by diluted acid washing, yielding HPGBs.

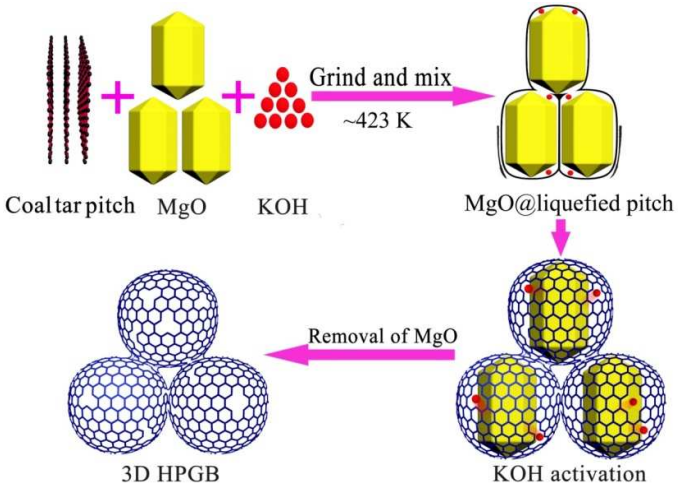


**Fig. 1** Schematic of direct fabrication process of 3D HPGB from coal tar pitch.

The TEM image of nano-MgO particles shows a rectangle projection with truncated morphology to some degree (**Fig. 2**a). The size of some MgO particles (circled by red circles) ranges from 85.0 to 100.0 nm. The FESEM image of $HPGB_{Ar}$ shows a thin carbon layer containing some mesopores and macropores (**Fig. 2**b). The size of some macropores also ranges from 85.0 to 100.0 nm, indicating that the macropores are inherited from the natural structure of MgO template. **Fig. 2**c and d is the TEM images of $HPGB_{Ar}$, showing that they are 3D hollow porous graphene balls, and some balls are open. The diameter of some graphene balls is similar to that of MgO particles, e.g. in a range of 85−100 nm, indicating that the size of graphene balls can be controlled by changing the diameter of MgO template. It can be seen that the thickness of the curved wall in opend graphene ball in **Fig. 2**d is below 1 nm. It is interesting to mention that a similar graphene-like stone ball under a monster in front of the Lama Temple in Beijing of China was designed and built as art decoration in 1694 in Qing dynasty (Supporting Information; Fig. S1), which seems to be made of a blown graphene sheet with only carbon six-member rings. **Fig. 2**e and f are the TEM images of $HPGB_{N2}$, showing that 3D hollow porous graphene balls are also fabricated in $N_2$ atmosphere, and the diameter of some graphene balls is almost equal to that of MgO particles. The wall thickness of the graphene ball in **Fig. 2**f is also below 1 nm. This means that the formation of

3D HPGBs are not sensitive to the gas atmosphere, and the production cost of HPGBs can be reduced by using cheap $N_2$ instead of argon. Besides, HPGBs ($HPGB_{NP-6}$ and $HPGB_{NP-4}$) can also be synthesized directly from coal tar pitch by a simple nano-MgO template strategy coupled with KOH activation at negative pressure from −0.05 to −0.10 MPa (Supporting Information; Fig. S2a and b). $HPGB_{2Ar}$ can be made from coal tar pitch by only using nano-MgO as template (Supporting Information; Fig. S2d). When nano-MgO template was not used, only conventional porous carbon, i.e. $PC_{1Ar}$, is obtained from coal tar pitch in the presence of KOH (Supporting Information; Fig. S2c).

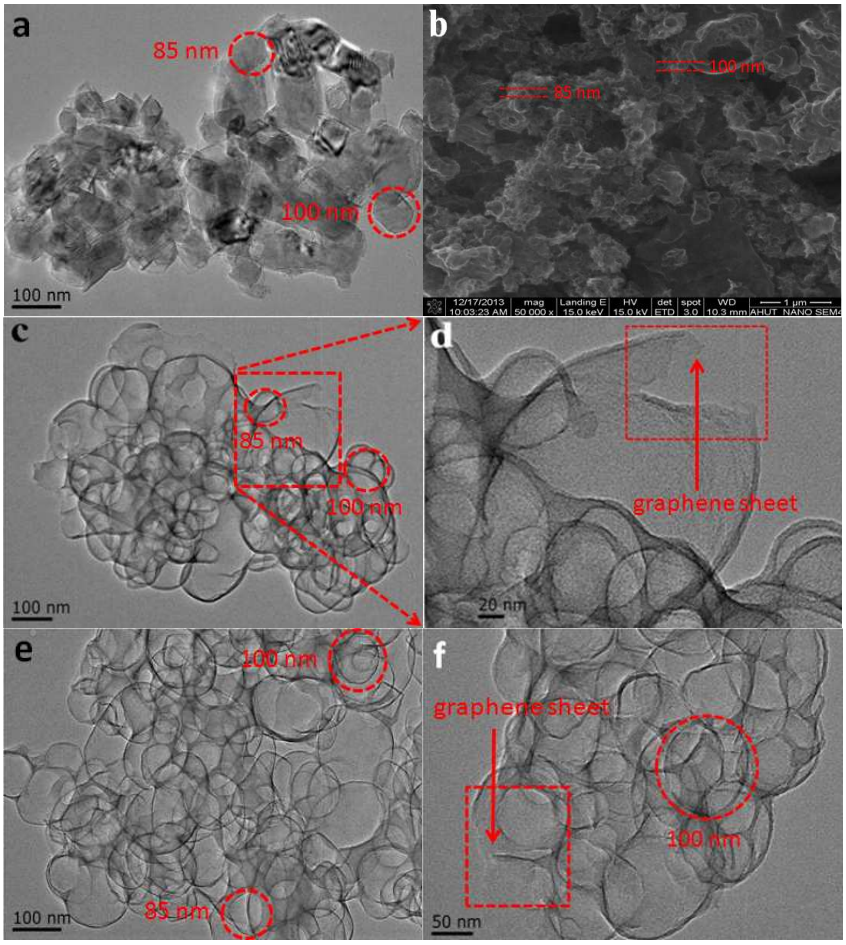


**Fig. 2** (a) TEM image of MgO particles; (b) FESEM image of $HPGB_{Ar}$; (c, d) TEM image of $HPGB_{Ar}$; (e, f) TEM images of $HPGB_{N2}$.

The $N_2$ adsorption-desorption isotherms of HPGBs are typical IV type isotherms with strong $N_2$ adsorption at low pressure and an obvious loop at relative pressure of 0.5−1.0, indicating the presence of micropore, mesopore and macropore in the HPGBs (**Fig. 3**a). The pore size distribution of HPGBs shows the micropores with a dual center at 0.6−0.7 and 1.2 nm, and macrospores centering at 118.0 nm, and continuous-distribution pores in a range of 35.0−95.0 nm (**Fig. 3**b). **Fig. 3**c is the cumulative pore volume of $HPGB_{Ar}$ and $HPGB_{N2}$, showing that their micropore volume is 57.7−58.3% with the remaining being mesopores and macropores of 41.7−42.3 %. The mesopores and macropores are beneficial for electrolyte ions to quickly go in and out of the micropores of the HPGBs. The TEM image of $HPGB_{Ar}$ (Supporting Information, Fig. S2e) may also provide some information about the micropores.

The pore structure parameters of the HPGBs are summarized in **Table 1**. The $S_{BET}$ of $HPGB_{Ar}$ with the highest yield of 67.3% is 1871 $m^2 g^{-1}$, which is slightly higher than 1832 $m^2 g^{-1}$ of $HPGB_{N2}$. The $S_{BET}$ of $HPGB_{NP-6}$ is the biggest among the HPGBs, reaching at 1947 $m^2 g^{-1}$ at a lower yield of 47.7 wt.%, which may be due to the low pressure shear force in the reaction step. The $S_{BET}$ of HPGBs decreases from 1947 ($HPGB_{NP-6}$) to 1858 $m^2 g^{-1}$ ($HPGB_{NP-4}$) when the mass ratio of MgO/pitch drops from 6 to 4 with other conditions remaining unchanged. Obviously, the $S_{BET}$ of HPGBs can be tuned by simply adjusting the mass ratio of MgO to pitch. It was reported that the $S_{BET}$ of PC made from coal tar pitch by only using needle-like nano-sized MgO as template reached 864 $m^2 g^{-1}$, of which MgO is produced *in situ* by decomposing $Mg(OH)_2$ via several steps including dissolving coal tar pitch in tertrahydrofuran (THF) and removing the THF insoluble fraction through filtration, and dispersing $Mg(OH)_2$ in ethanol as well as the stabilization and carbonization of the mixture of coal tar pitch and $Mg(OH)_2$.[26] Obviously, the $S_{BET}$ of HPGB made by a simple nano-MgO template strategy coupled with KOH activation in our case is 2.12 times higher than that made by only using nano-sized MgO as template.[26] The KOH dosage in present work is relatively low, i.e. the KOH/pitch mass ratios are not bigger than 2. In other words,

plentiful pores can be easily formed in the shells of HPGBs due to the efficient activation of KOH to the thin carbon coating layer.

**Table 1** Pore structure parameters of HPGBs in different yields

| Samples | $D_{ap}$ (nm) | $S_{BET}$ ($m^2\ g^{-1}$) | $S_{mic}$ ($m^2\ g^{-1}$) | $V_t$ ($cm^3\ g^{-1}$) | $V_{mic}$ ($cm^3\ g^{-1}$) | $V_{meso}$ ($cm^3\ g^{-1}$) | Yield (wt.%) |
|---|---|---|---|---|---|---|---|
| $HPGB_{Ar}$ | 2.31 | 1871 | 1761 | 1.08 | 0.79 | 0.29 | 67.3 |
| $HPGB_{N2}$ | 2.48 | 1832 | 1643 | 1.14 | 0.72 | 0.42 | 57.3 |
| $HPGB_{NP-6}$ | 2.39 | 1947 | 1768 | 1.16 | 0.76 | 0.40 | 47.7 |
| $HPGB_{NP-4}$ | 2.39 | 1858 | 1693 | 1.10 | 0.76 | 0.34 | 48.3 |
| $PC_{1Ar}$ | 1.86 | 1720 | 1691 | 0.80 | 0.77 | 0.03 | 59.2 |
| $HPGB_{2Ar}$ | 10.66 | 512 | 109 | 1.36 | 0.05 | 1.31 | 43.7 |

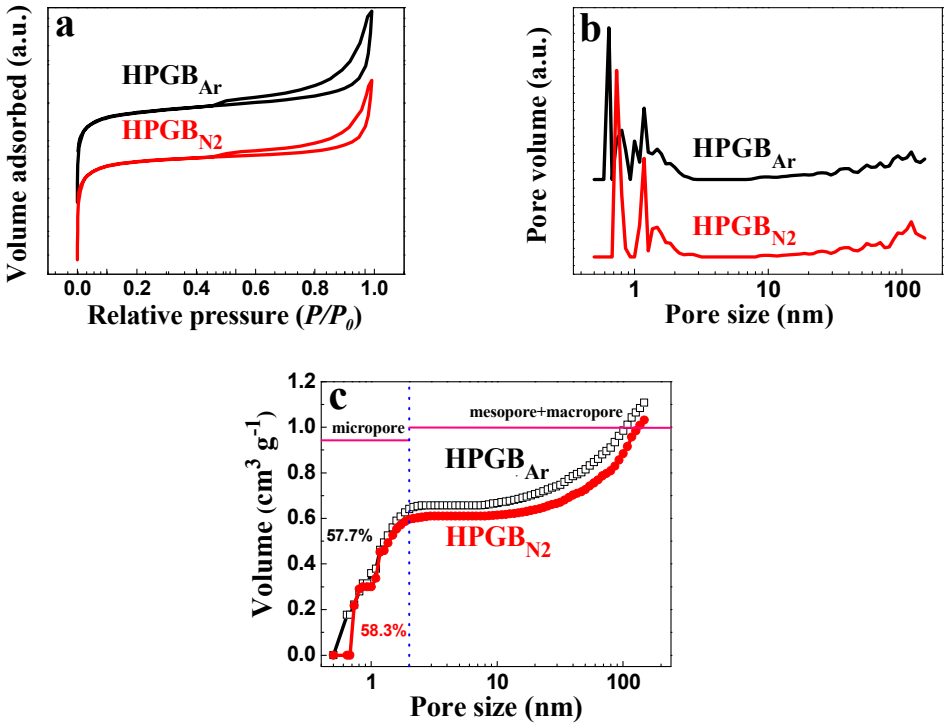


**Fig. 3** (a) Nitrogen adsorption-desorption isotherms; (b) pore size distribution; and (c) cumulative pore volume of $HPGB_{Ar}$ and $HPGB_{N2}$.

The XPS analysis shows that no impurities are observed in $HPGB_{Ar}$ (**Fig. 4**a). The TG results show that the ash content in HPGBs is below 1.0 wt.%. **Fig. 4**b is the Mg1s spectra of MgO, MgO@$HPGB_{Ar}$ and $HPGB_{Ar}$, in which the peaks of Mg1s in MgO and MgO@$HPGB_{Ar}$ center at the same binding energy of 1304.0 eV. **Fig. 4**c is the O1s spectra of MgO, MgO@$HPGB_{Ar}$ and $HPGB_{Ar}$, in which the peaks of O1s in MgO and MgO@$HPGB_{Ar}$ center at 531.1 eV. These XPS results indicate that no chemical bonds are formed between carboxylic acid group ($COO^-$) and nano-MgO. The oxygen-containing groups including C=O, C−OH and COOH (**Fig. 4**d) are formed on the shells of HPGBs due to the efficient KOH activation to the thin carbonaceous layers coated outside the MgO template. The contents of oxygen-containing groups including C=O, C−OH, COOH in HPGBs are calculated based on the XPS results (**Table 2**), showing that the O1s content in $HPGB_{Ar}$, $HPGB_{N2}$, $HPGB_{NP-6}$ and $HPGB_{NP-4}$ drops from 17.4 to 12.2%. N-species (≈396 eV, N1s) are not observable in $HPGB_{Ar}$, $HPGB_{N2}$, $HPGB_{NP-6}$ and $HPGB_{NP-4}$ (Supporting Information; Fig. S3), showing that the working $N_2$ gas atmosphere is not involved in the chemcial reactions related to HPGBs.

**Table 2** Contents of carbon and oxygen elements in HPGBs.

| Samples | C1s (%) | O1s (%) | O1s | | |
|---|---|---|---|---|---|
| | | | C=O (%) | C−OH (%) | COOH (%) |
| $HPGB_{Ar}$ | 82.6 | 17.4 | 6.5 | 10.5 | 0.4 |
| $HPGB_{N2}$ | 83.8 | 16.2 | 7.2 | 8.9 | 0.2 |
| $HPGB_{NP-6}$ | 86.2 | 13.8 | 5.3 | 7.4 | 1.1 |
| $HPGB_{NP-4}$ | 87.8 | 12.2 | 3.8 | 5.4 | 3.1 |

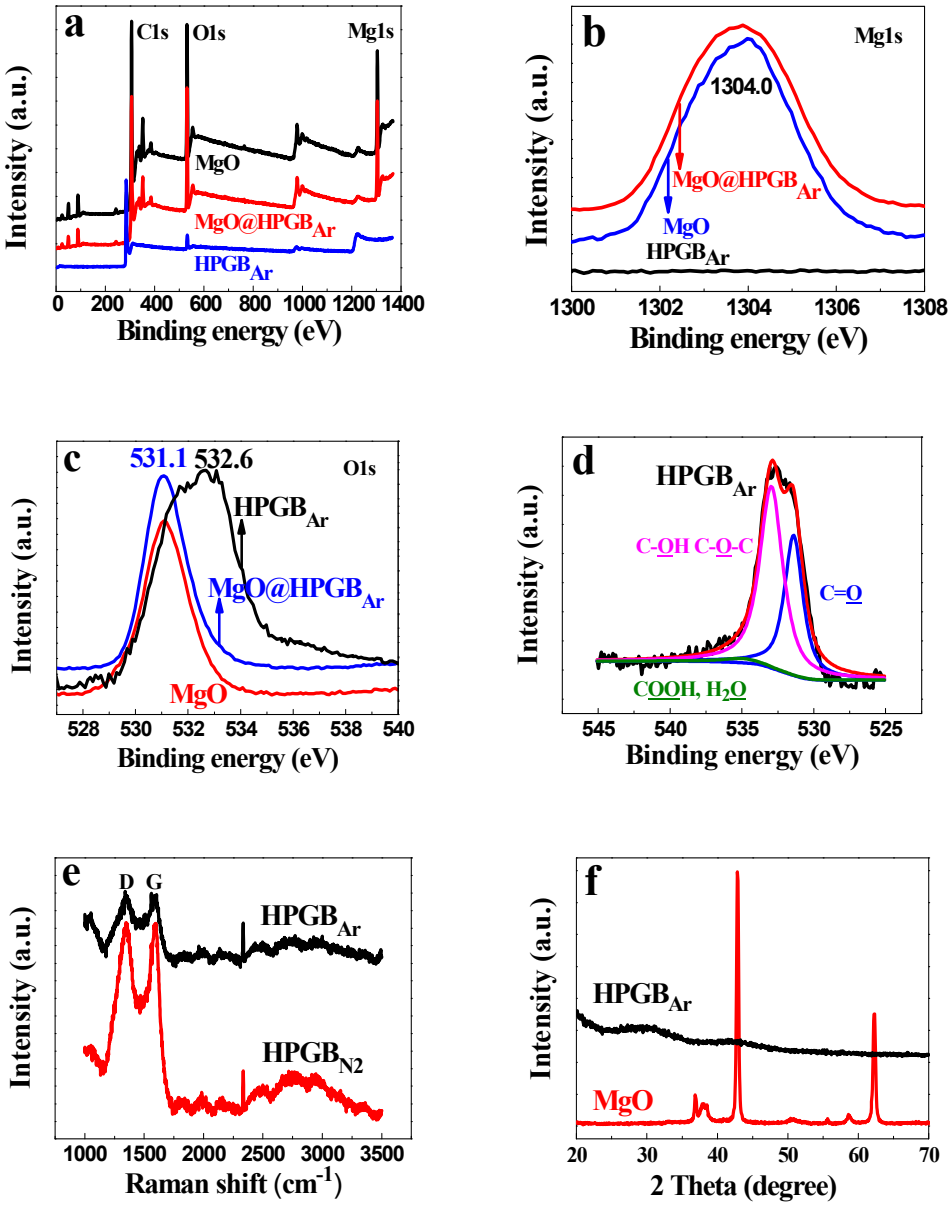


**Fig. 4** (a) XPS spectra of $HPGB_{Ar}$; (b) Mg1s and (c) O1s spectra of MgO, $MgO@HPGB_{Ar}$ and $HPGB_{Ar}$; (d) O1s spectra of $HPGB_{Ar}$; (e) Raman spectra of $HPGB_{Ar}$ and $HPGB_{N2}$; (f) XRD patterns of $HPGB_{Ar}$ and MgO.

The Raman spectra of $HPGB_{Ar}$ and $HPGB_{N2}$ show the well-known D-band at ~1320 $cm^{-1}$ and G-band at ~1590 $cm^{-1}$ (**Fig. 4**e). The strong D-band indicates that the as-made HPGBs have a low graphitization degree, and a significant amount of disordered structure and defects,

which may be resulted from the KOH activation. The XRD pattern of the $HPGB_{Ar}$ does not show sharp peaks, indicative of the amorphous structure of the $HPGB_{Ar}$ (**Fig. 4**f). The comparison of the XRD patterns of $HPGB_{Ar}$ and MgO template in **Fig. 4**f confirms that the MgO template can be easily removed by diluted acid washing, yielding high-purity HPGBs. In our experiment, about 84.0 wt.% of Mg are recovered by chemical precipitation via the formation of $MgCO_3$ ($Mg^{2+}+CO_3^{2-}\leftrightarrow MgCO_3$) by adding $Na_2CO_3$ solution to the $Mg^{2+}$-containing solution, i.e. MgO can be recycled after the decomposition of $MgCO_3$ for the synthesis of HPGBs.

The galvanostatic charge-discharge curve of $HPGB_{Ar}$ at 2 A $g^{-1}$ is symmetrical without obvious pseudocapacitance behavior of functional groups, and the IR drop of $HPGB_{Ar}$ is only 0.0076 V (**Fig. 5**a). The internal resistance of the single $HPGB_{Ar}$ electrode at 2 A $g^{-1}$ is very small, only 0.20 Ohm, due to both the good electronic conductivity and fast diffusion of electrolyte ions. **Fig. 5**b is the specific capacitance of HPGB electrodes in 6M KOH electrolyte at varying discharge current density. The specific capacitance of $HPGB_{Ar}$ and $HPGB_{N2}$ reaches 321 F $g^{-1}$ (17.2 μF $cm^{-2}$) and 306 F $g^{-1}$ (16.7 μF $cm^{-2}$) at 0.05 A $g^{-1}$, respectively, and it is 286 F $g^{-1}$ (15.3 μF $cm^{-2}$) and 275 F $g^{-1}$ (15.0 μF $cm^{-2}$) at 0.2 A $g^{-1}$. The specific capacitance of $HPGB_{Ar}$ and $HPGB_{N2}$ remains at 254 F $g^{-1}$ and 237 F $g^{-1}$ at 10 A $g^{-1}$. At 20 A $g^{-1}$ (a current density increase by a factor of 400), the specific capacitance of $HPGB_{Ar}$ and $HPGB_{N2}$ remains at 244 F $g^{-1}$ and 234 F $g^{-1}$, respectively. At 10 A $g^{-1}$ and 20 A $g^{-1}$, the capacitance retention of $HPGB_{Ar}$ is 79.1% and 76.0%, respectively, while for $HPGB_{N2}$, it is 77.5% and 76.5%. It is interesting to note that the nanoscale thickness of HPGB shells is favorable for fast diffusion of electrolyte ions, resulting in low ion-transport resistance due to the unique porous structure of HPGBs with well-developed mesoporous channels and a short diffusion distance. Moreover, thinner shells of the HPGBs not only function as electrolyte ion buffering reservoir but also facilitate the collection and transport of electrons during the cycle charge-discharge process. The capacitance retention of the $HPGB_{Ar}$

electrode at 0.1 A $g^{-1}$ is 94.5%, while for $HPGB_{N2}$, it is 94.4% of the initial capacitance in 6 M KOH electrolyte after 1000 charge-discharge cycles (**Fig. 5**c). This is indicative of good electrochemical stability and excellent reversibility of the HPGB electrodes. It was reported that the specific capacitance of high charge-density nanoparticles with near spherical shape reached 277 F $g^{-1}$ at 0.2 A $g^{-1}$ in 6 M KOH electrolyte.[27] The specific capacitance of carbon nanocages made from benzene reached 178 F $g^{-1}$,[28] while for $Ni(OH)_2$/graphene//porous graphene, it was 220 F $g^{-1}$ at 10 A $g^{-1}$ in 6 M KOH electrolyte.[29] It should bear in mind that coal tar pitch, the carbon source of HPGB in present work, is much cheaper than benzene. For nitrogen-rich networks, the specific capacitance reached 173 F $g^{-1}$ at 10 A $g^{-1}$,[30] while for hierarchical carbide-derived carbon foams, it was 175 F $g^{-1}$ at 20 A $g^{-1}$ in 1 M $H_2SO_4$ electrolyte.[31] For functionalized 3D hierarchical porous carbon, the specific capacitance reached 192 F $g^{-1}$,[32] while for human hair-derived carbon flakes, it was 227 F $g^{-1}$ at 10 A $g^{-1}$ in 6 M KOH electrolyte.[33] For porous graphene made with flake-like MgO as template and ferrocene as the carbon precursor, the specific capacitance was 196 F $g^{-1}$ at 10 A $g^{-1}$.[34] Obviously, the $HPGB_{Ar}$ with high specific capacitance, excellent rate performance and good cycle stability in our present work is very attractive as the eletrode of supercapacitors. It was reported that the specific capacitance of porous carbon made from a resorcinol/formaldehyde-based organic aquagel by introducing needle-like nano-sized $Mg(OH)_2$ into the reaction system reached 187 F $g^{-1}$ at 0.2 A $g^{-1}$.[35] For the conventional mesoporous carbons made from coal tar pitch by coupling KOH activation with a MgO template, the specific capacitance was only 227 F $g^{-1}$ at 0.05 A $g^{-1}$.[36] For porous carbons made from deoiled asphalt by the combination of nano-sized MgO template and NaOH activation, the specific capacitance reached 74 F $g^{-1}$ at 10 A $g^{-1}$.[37] For the nitrogen-enriched hierarchical porous carbon made from melamine-formaldehyde resin/poly(vinyl alcohol) blend using MgO as template, the specific capacitance was 224 F $g^{-1}$ at 0.05 A $g^{-1}$.[38] For the $HPGB_{Ar}$ and $HPGB_{N2}$ in the present work, the volumetric capacitance reached 114 F $cm^{-3}$ and 134 F $cm^{-3}$ at 0.8 A $g^{-1}$ in 6

M KOH electrolyte, respectively, which is based on that the bulk density of $HPGB_{Ar}$ and $HPGB_{N2}$ is 0.42 g $cm^{-3}$ and 0.51 g $cm^{-3}$. It was reported that the volumetric capacitance of ionic liquid $C_{16}mimBF_4$ assisted synthesis of poly(benzoxazine-co-resol)-based hierarchically porous carbons was 101 F $cm^{-3}$ at 0.5 A $g^{-1}$ in 6 M KOH electrolyte.[39] The volumetric capacitance of the MOF-derived nanoporous carbons in 6 M KOH electrolyte ranged from 81 to 165 F $cm^{-3}$.[40] In comparison to the porous carbon materials reported in literature, HPGBs directly made from coal tar pitch in our presetn work hold promise as high performance electrode materials for supercapacitors in terms of cheap raw materials, simple synthesis method, 3D hollow ball-like morphology with a porous thin shell, short transfer distance of electrolyte ions, high capacitance, good rate performance and cycle stability.

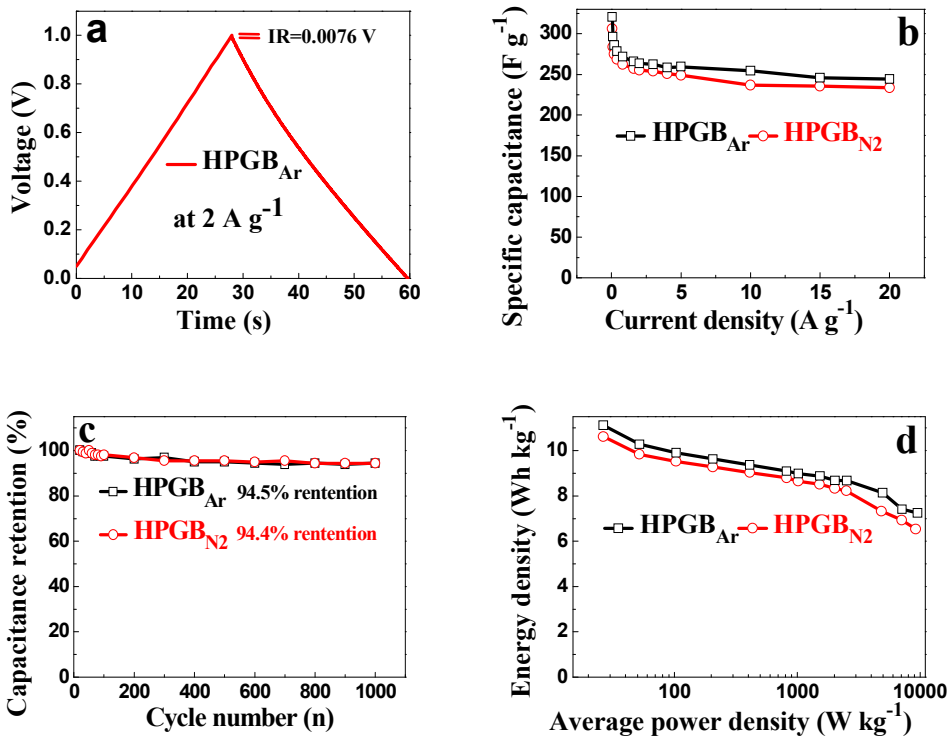


**Fig. 5** (a) Charge-discharge curve of $HPGB_{Ar}$ electrodes in 6 M KOH electrolyte at 2 A $g^{-1}$; (b) specific capacitance of HPGB electrodes at different discharge current density; (c) capacitance retention of HPGB electrodes at 0.1 A $g^{-1}$; (d) Ragone plots of HPGB capacitors.

**Fig. 5**d shows the Ragone plots of supercapacitors made of HPGBs. The energy density of the $HPGB_{Ar}$ capacitor is 11.12 Wh $kg^{-1}$ (4.67 Wh $L^{-1}$) at 0.05 A $g^{-1}$, and 7.25 Wh $kg^{-1}$ (3.05 Wh $L^{-1}$) at 20 A $g^{-1}$, while for the $HPGB_{N2}$ capacitor, it is 10.62 Wh $kg^{-1}$ (5.41 Wh $L^{-1}$) at 0.05 A $g^{-1}$ and 6.54 Wh $kg^{-1}$ (3.34 Wh $L^{-1}$) at 20 A $g^{-1}$. The $HPGB_{Ar}$ capacitor renders a higher energy density and energy density retention (65.2%) than the $HPGB_{N2}$ capacitor (61.6%), maybe due to the higher $S_{BET}$ of the $HPGB_{Ar}$ and more mesopores and macropores (42.3%).

**Fig. 6**a is the CV curves of the $HPGB_{Ar}$ electrode at scan rates from 2 to 500 mV $s^{-1}$, in which the nearly perfect symmetric rectangular shapes at higher scan rates are indictive of the excellent rate performance of the HPGB electrodes and the formation of perfect electrical double layers due to the reversible adsorption and desorption of the electrolyte ions. The symmetric rectangular shape of the $HPGB_{N2}$ electrode at 500 mV $s^{-1}$ also proves its excellent rate performance (**Fig. 6**b). The specific capacitance of the $HPGB_{Ar}$ electrode and $HPGB_{N2}$ electrode calculated from the CV curves at 100 mV $s^{-1}$ reaches 225 F $g^{-1}$ (12.0 μF $cm^{-2}$) and 218 F $g^{-1}$ (11.3 μF $cm^{-2}$), respectively, as shown in **Table 3**. At 200 mV $s^{-1}$, they are 211 F $g^{-1}$ (11.9 μF $cm^{-2}$) and 201 F $g^{-1}$ (11.0 μF $cm^{-2}$).

**Table 3** Specific capacitance of the HPGBs at different scan rates

| Samples | Specific capacitance (F $g^{-1}$) at different scan rates (mV $s^{-1}$) | | | | | | | |
|---|---|---|---|---|---|---|---|---|
| | **2** | **5** | **10** | **25** | **50** | **100** | **200** | **500** |
| $HPGB_{Ar}$ | 260 | 256 | 252 | 243 | 235 | 225 | 211 | 174 |
| $HPGB_{N2}$ | 254 | 250 | 245 | 236 | 228 | 218 | 201 | 161 |
| $HPGB_{NP-6}$ | 224 | 224 | 221 | 213 | 207 | 198 | 186 | 157 |

**Fig. 6**c is the Nyquist plots of the HPGB electrodes. The short x-intercept (0.16−0.22 Ohm), negligible diameter of the semicircle and high slope at low frequency reveal that the HPGB electrodes have very low internal resistance and charge-discharge resistance, and excellent pore accessibility for the electrolyte ions. **Fig. 6**d is the specific capacitance of the

HPGB electrodes at different frequency. The maximum capacitance occurs at the lowest frequency of 0.001 Hz, with a value of 280 F $g^{-1}$ (15.0 μF $cm^{-2}$) for $HPGB_{Ar}$ and 240 F $g^{-1}$ (13.1 μF $cm^{-2}$) for $HPGB_{N2}$. At 1.0 Hz, the capacitance of the $HPGB_{Ar}$ remains at 246 F $g^{-1}$ while it is 214 F $g^{-1}$ for the $HPGB_{N2}$. At 50.0 Hz, it is 73 F $g^{-1}$ for $HPGB_{Ar}$, while it is 44 F $g^{-1}$ for $HPGB_{N2}$. It was once reported that the capacitance of hierarchical porous carbons made from direct coal liquefaction residue and cetyltrimethylammonium bromide was about 150 F $g^{-1}$ at 1.0 Hz in 6 M KOH electrolyte while the capacitance dropped to below 30 F $g^{-1}$ at frequency over 50.0 Hz.[41]

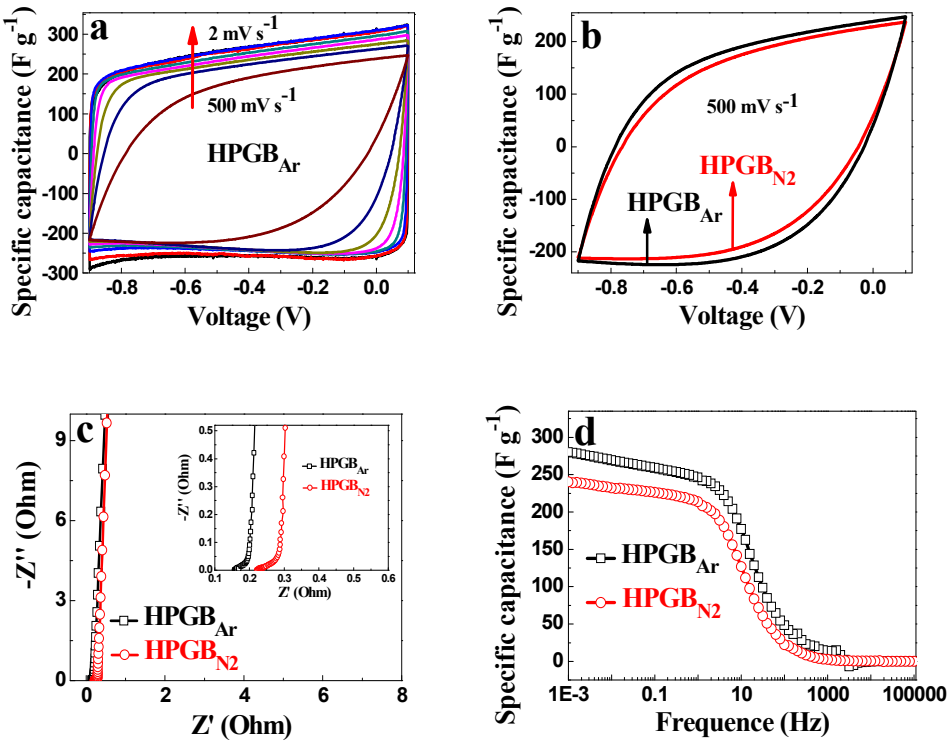


**Fig. 6** (a) CV curves of $HPGB_{Ar}$ electrodes at scan rates from 2 to 500 mV $s^{-1}$; (b) CV curves of HPGB electrodes at 500 mV $s^{-1}$; (c) Nyquist plots of HPGB electrodes; (d) specific capacitance of HPGB electrodes at different frequency.

The results discussed above have demonstrated that the HPGBs hold promise as electrode materials for supercapacitors, evidenced by their superior energy storage performance due to

their high specific surface area, and unique 3D hollow porous ball-like texture with thin shells that are rich of well-balanced pore structure. The 3D carbon shells in the HPGBs resulted from polycyclic aromatic hydrocarbon molecules in coal tar pitch help to greatly improve the conductivity of electrons. The macropores, mesopores and micropores in the thin carbon shells of HPGBs provide abundant channels and active sites for fast transportation and storage of electrolyte ions. The short diffusion distance in the thin HPGB shells reduces the ion transfer resistance. These three factors combine together to make the HPGBs have high capacitance and excellent rate performance.

## Conclusions

Novel HPGBs with thin ball shells have been directly synthesized from coal tar pitch by coupling MgO-template and KOH chemical activation. The porous carbon networks with a balanced pore distribution in the shells of HPGBs help to improve the conductivity of electrons, and to reduce the ion transfer resistance because of the abundant porous channels and active sites in the thin carbon shells for fast transportation and storage of electrolyte ions. Because of these synergistic features, the HPGBs show a high capacitance of 321 F $g^{-1}$ at 0.05 A $g^{-1}$, an excellent rate performance of 244 F $g^{-1}$ at 20 A $g^{-1}$ and good cycle stability. This method may pay a new way for the efficient large-scale production of low-cost HPGBs as electrode materials for energy storage.

## Acknowledgements

This work was partly supported by the NSFC (Nos. 50802002, 51272004, U1361110 and 21336001), and the Program for New Century Excellent Talents of the Education Ministry of China (No. NCET−13−0643).

**Notes and references**

(1) C. R. Pérez, S. H. Yeon, J. Ségalini, V. Presser, P. L. Taberna, P. Simon and Y. Gogotsi, *Adv. Funct. Mater.*, 2013, **23**, 1081−1089.

(2) J. Yan, Q. Wang, T. Wei and Z. J. Fan, *Adv. Energy Mater.*, 2014, DOI: 10.1002/aenm.201470017.

(3) F. Liu, S. Y. Song, D. F. Xue and H. J. Zhang, *Adv. Mater.*, 2012, **24**, 1089−1094.

(4) M. R. Lukatskaya, O. Mashtalir, C. E. Ren, Y. Dallagnes, P. Rozier, P. L. Taberna, M. Naguib, P. Simon, M. W. Barsoum and Y. Gogosti, *Science*, 2013, **341**, 1502−1505.

(5) S. Kondrat, C. R. Pérez, V. Presser, Y. Gogotsi and A. A. Kornyshev, *Energy Environ. Sci.*, 2012, **5**, 6474−6479.

(6) S. Stankovich, D. A. Dikin, G. H. B. Dommett, K. M. Kohlhaas, E. J. Zimney, E. A. Stach, R. D. Piner, S. B. T. Nguyen and R. S. Ruoff, *Nature*, 2006, **442**, 282−286.

(7) M. F. El-Kady, V. Strong, S. Dubin and R. B. Kaner, *Science*, 2012, **335**, 1326−1330.

(8) Z. S. Wu, Y. Sun, Y. Z. Tan, S. B. Yang, X. L. Feng and K. Müllen, *J. Am. Chem. Soc.*, 2012, **134**, 19532−19535.

(9) Z. S. Wu, A. Winter, L. Chen, Y. Sun, A. Turchanin, X. L. Feng and K. Müllen, *Adv. Mater.*, 2012, **24**, 5130−5135.

(10) Z. S. Wu, S. B. Yang, Y. Sun, K. Parvez, X. L. Feng and K. Müllen, *J. Am. Chem. Soc.*, 2012, **134**, 9082−9085.

(11) S. Han, D. Q. Wu, S. Li, F. Zhang and X. L. Feng, *Adv. Mater.*, 2014, **26**, 849−864.

(12) C. J. Cui, W. Z. Qian, Y. T. Yu, C. Y. Kong, B. Yu, L. Xiang and F. Wei, *J. Am. Chem. Soc.*, 2014, **136**, 2256−2259.

(13) J. J. Liu, W. Lv, W. Wei, C. Zhang, Z. J. Li, B. H. Li, F. Y. Kang and Q. H. Yang, *J. Mater. Chem. A*, 2014, **2**, 3031−3037.

(14) Y. W. Zhu, S. Murali, M. D. Stoller, K. J. Ganesh, W. W. Cai, P. J. Ferreira, A. Pirkle, R. M. Wallace, K. A. Cychosz, M. Thommes, D. Su, E. A. Stach and R. S. Ruoff, *Science*,

2011, **332**, 1537−1541.

(15) X. M. Fan, C. Yu, J. Yang, Z. Ling and J. S. Qiu, *Carbon*, 2014, **70**, 130−141.

(16) L. Jiang, T. C. Niu, X. Q. Lu, H. L. Dong, W. Chen, Y. Q. Liu, W. P. Hu and D. B. Zhu, *J. Am. Chem. Soc.*, 2013, **135**, 9050−9054.

(17) L. Talirz, H. Söde, J. M. Cai, P. Ruffieux, S. Blankenburg, R. Jafaar, R. Berger, X. L. Feng, K. Müllen, D. Passerone, R. Fasel and C. A. Pignedoli, *J. Am. Chem. Soc.*, 2013, **135**, 2060−2063.

(18) Y. Fang, Y. Y. Lv, R. C. Che, H. Y. Wu, X. H. Zhang, D. Gu, G. F. Zheng and D. Y. Zhao, *J. Am. Chem. Soc.*, 2013, **135**, 1524−1530.

(19) Y. Y. Li, Z. S. Li and P. K. Shen, *Adv. Mater.*, 2013, **25**, 2474−2480.

(20) D. L. Wertz and M. Bissell, *Energy Fuels*, 1994, **8**, 613−617.

(21) H. Aso, K. Matsuoka, A. Sharma and A. Tomita, *Energy Fuels*, 2004, **18**, 1309−1314.

(22) X. J. He, N. Zhao, J. S. Qiu, N. Xiao, M. X. Yu, C. Yu, X. Y. Zhang and M. D. Zheng, *J. Mater. Chem. A*, 2013, **1**, 9440−9448.

(23) Q. Zhou, Z. B. Zhao, Y. T. Zhang, B. Meng, A. N. Zhou and J. S. Qiu, *Energy Fuels*, 2012, **26**, 5186−5192.

(24) G. Q. Ning, C. G. Xu, X. Zhu, R. F. Zhang, W. Z. Qian, F. Wei, Z. J. Fan and J. S. Gao, *Carbon*, 2013, **56**, 38−44.

(25) L. L. Zhang, X. Zhao, H. X. Ji, M. D. Stoller, L. F. Lai, S. Murali, S. Mcdonnell, B. Cleveger, R. M. Wallace and R. S. Ruoff, *Energy Environ. Sci.*, 2012, **5**, 9618−9625.

(26) W. F. Zhang, Z. H. Huang, G. P. Cao, F. Y. Kang and Y. S. Yang, *J. Phys. Chem. Solids*, 2012, **73**, 1428–1431.

(27) N. D. Kim, D. Bruce Buchholz, G. Casillas, M. José-Yacaman and R. P. H. Chang, *Adv. Funct. Mater.*, 2014, DOI: 10.1002/adfm.201304130.

(28) K. Xie, X. T. Qin, X. Z. Wang, Y. N. Wang, H. S. Tao, Q. Wu, L. J. Yang and Z. Hu, *Adv. Mater.*, 2012, **24**, 347−352.

(29) J. Yan, Z. J. Fan, W. Sun, G. Q. Ning, T. Wei, Q. Zhang, R. F. Zhang, L. J. Zhi and F. Wei, *Adv. Funct. Mater.*, 2012, **22**, 2632−2641.

(30) L. Hao, B. Luo, X. L. Li, M. H. Jin, Y. Fang, Z. H. Tang, Y. Y. Jia, M. H. Liang, A. Thomas, J. H. Yang and L. J. Zhi, *Energy Environ. Sci.*, 2012, **5**, 9747−9751.

(31) M. Oschatz, L. Borchardt, K. Pinkert, S. Thieme, M. R. Lohe, C. Hoffmann, M. Benusch, F. M. Wisser, C. Ziegler, L. Giebeler, M. H. Rümmeli, J. Eckert, A. Eychmüller and S. Kaskel, *Adv. Energy Mater.*, 2013, DOI: 10.1002/aenm.201300645.

(32) L. Qie, W. M. Chen, H. H. Xu, X. Q. Xiong, Y. Jiang, F. Zou, X. L. Hu, Y. Xin, Z. L. Zhang and Y. H. Huang, *Energy Environ. Sci.*, 2013, **6**, 2497−2504.

(33) W. J. Qian, F. X. Sun, Y. H. Xu, L. H. Qiu, C. H. Liu, S. D. Wang and F. Yan, *Energy Environ. Sci.*, 2014, **7**, 379−386.

(34) H. J. Wang, X. X. Sun, Z. H. Liu and Z. B. Lei, *Nanoscale*, 2014, **6**, 6577–6584.

(35) W. F. Zhang, Z. H. Huang, C. J. Zhou, G. P. Cao, F. Y. Kang and Y. S. Yang, *J. Mater. Chem.*, 2012, **22**, 7158–7163.

(36) X. J. He, R. C. Li, J. S. Qiu, K. Xie, P. H. Ling, M. X. Yu, X. Y. Zhang and M. D. Zheng, *Carbon*, 2012, **50**, 4911–4921.

(37) W. F. Zhang, Z. H. Huang, Z. Guo, C. Li, and F. Y. Kang, *Mater. Lett.*, 2010, **64**, 1868–1870.

(38) C. Ma, J. L. Shi, Y. Song, D. Q. Zhang, X. L. Zhai, M. Zhong, Q. G. Guo and L. Liu, *Int. J. Electrochem. Sci.*, 2012, **7**, 7587–7599.

(39) D. C. Guo, J. Mi, G. P. Hao, W. Dong, G. Xiong, W. C. Li and A. H. Lu, *Energy Environ. Sci.*, 2013, **6**, 652–659.

(40) W. Chaikittisilp, K. Ariga and Y. Yamauchi, *J. Mater. Chem. A*, 2013, **1**, 14–19.

(41) J. B. Zhang, L. J. Jin, J. Cheng and H. Q. Hu, *Carbon*, 2013, **55**, 221−232.

**Graphical Abstract**

**All Authors**: Xiaojun He*, Hebao Zhang, Hao Zhang, Xiaojing Li, Nan Xiao and Jieshan Qiu*

**Keywords**: 3D porous graphene ball; direct synthesis; supercapacitor; high capacitance

**Title:** Direct synthesis of 3D hollow porous graphene balls from coal tar pitch for high performance supercapacitors

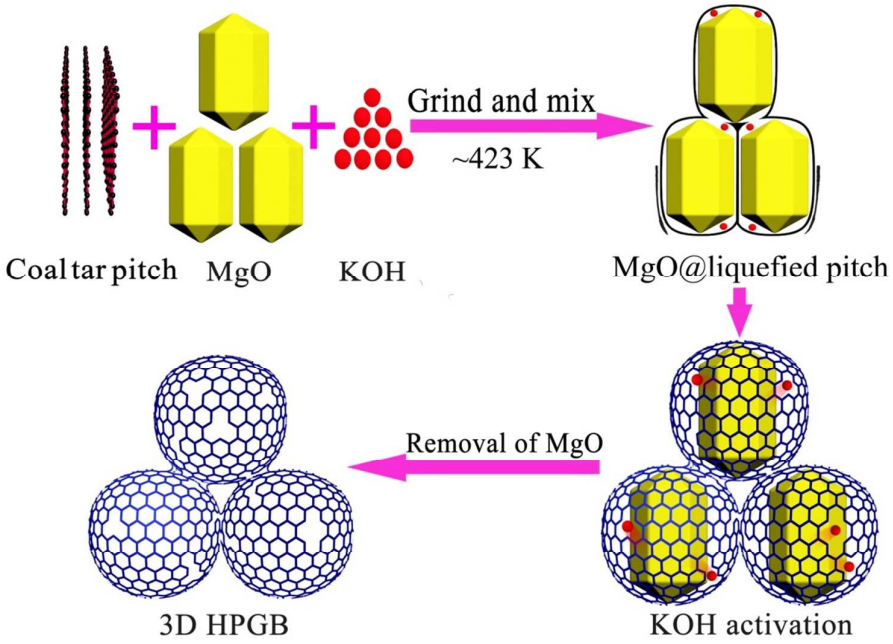


**A simple and effective method for direct synthesis of hollow porous graphene balls (HPGBs) for high performance supercapacitors.**